ADVANCED PHOTONICS RESEARCH Open Access

www.adpr-journal.com

Liquid-Metal Fabrication of Ultrathin Gallium Oxynitride Layers with Tunable Stoichiometry

Panteha Pedram, Ali Zavabeti, Nitu Syed, Amine Slassi, Chung Kim Nguyen, Benjamin Fornacciari, Anne Lamirand, Jules Galipaud, Arrigo Calzolari, Régis Orobtchouk, Andreas Boes, Torben Daeneke, Sébastien Cueff, Arnan Mitchell, and Christelle Monat*

The synthesis of nanometer-thick (≈3 nm) gallium oxynitride (GaO_xN_y) layers with a variable stoichiometry is reported. The approach primarily exploits the liquid metal chemistry (LMC) technique and promises easier integration of 2D materials onto photonic devices compared to traditional top-down and bottom-up methods. The fabrication follows a two-step process, involving first liquid metal-based printing of a nanometer-thick layer of gallium oxide (Ga_2O_3), followed a plasma-enhanced nitridation reaction. Control over nitridation parameters (plasma power, exposure time) allows adjustment of the GaO_xN_y layer's composition, granting access to compounds with distinct optical properties (e.g., a 20% index variation), as demonstrated by ellipsometry and density functional theory (DFT) simulations. DFT provides a microscopic understanding of the effect of the bond polarization and crystallinity on the optical properties of GaO_xN_y compounds. These findings expand the knowledge of ultrathin GaO_xN_y alloys, which are poorly studied with respect to their gallium nitride (GaN) and Ga_2O_3 counterparts. They also represent an essential step toward integrating such 2D materials into photonic chips and offer new opportunities to improve the performance of hybrid optoelectronic devices.

1. Introduction

Since the isolation of graphene in 2004, several other atomically thin materials, referred to as 2D materials[1,2] have emerged, offering new optoelectronic properties,[3–10] which can complement silicon photonics.[11–13] Incorporating 2D materials into silicon-based devices has several potential advantages, for instance, the enhancement of light absorption[10] or the improvement of light emission efficiency.[14,15] Although the design of the underlying dielectric photonic devices can be optimized to enhance the low-light–matter interaction with these ultra-thin materials, their integration into host devices remains a technological challenge that depends on both the material and the host device. Developing new fabrication techniques for 2D materials, wherein integration and synthesis could be seamlessly achieved and independently of the host substrate, would greatly

P. Pedram, B. Fornacciari, A. Lamirand, R. Orobtchouk, S. Cueff, C. Monat
Institut des Nanotechnologies de Lyon
UMR CNRS
Ecole Centrale de Lyon
Université de Lyon
36 Av. Guy de Collongue, 69130 Écully, France
E-mail: Panteha.Pedram@ec-lyon.fr

P. Pedram, C. K. Nguyen, A. Boes, T. Daeneke, A. Mitchell
School of Engineering
RMIT University
124 La Trobe St, Melbourne, VIC 3001, Australia

A. Zavabeti
Department of Chemical Engineering
The University of Melbourne
Parkville, VIC 3010, Australia

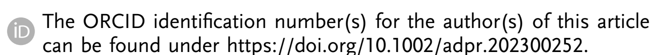
The ORCID identification number(s) for the author(s) of this article can be found under https://doi.org/10.1002/adpr.202300252.

© 2023 The Authors. Advanced Photonics Research published by Wiley-VCH GmbH. This is an open access article under the terms of the Creative Commons Attribution License, which permits use, distribution and reproduction in any medium, provided the original work is properly cited.

DOI: 10.1002/adpr.202300252

N. Syed
School of Physics
The University of Melbourne
Parkville, VIC 3010, Australia

A. Slassi, A. Calzolari
CNR-NANO Istituto Nanoscienze
I-41125 Modena, Italy

J. Galipaud
Laboratory of Tribology and System Dynamics
Ecole Centrale de Lyon
Université de Lyon
36 Av. Guy de Collongue, 69130 Écully, France

A. Boes
Institute for Photonics and Advanced Sensing
The University of Adelaide
Adelaide, SA 5005, Australia

A. Boes
School of Electrical and Mechanical Engineering
The University of Adelaide
Adelaide, SA 5005, Australia

facilitate the development of hybrid optoelectronic devices. Among 2D materials, Ga_2O_3 and GaN stand out due to their interesting optoelectronic properties.

Wide-bandgap Ga_2O_3 films have found applications in electronics,[16] photonics,[17] sensing,[18] resistive switching,[19] and bioinspired technologies.[20] Moreover, liquid gallium serves as a solvent with promising potential for growing metallic crystals at the nanoscale.[21] Additionally, a study by Mayyas. M, et al. demonstrated the direct expulsion of metals from Ga-based alloys (GaSn, GaIn, and GaZn) by inducing interfacial perturbations through electrochemistry.[22] This concept can be applied to process liquid alloys, offering a method for producing metallic nanostructures with broad applications. Recently, research on 2D surface oxide films of liquid gallium alloys has been set up to realize economically affordable techniques for synthesizing and extracting high-quality 2D semiconductors.[23] The choice of the synthesis technique profoundly impacts the morphology, the phase, and, therefore, the Ga_2O_3 electronic structure.[24–29] Many liquid-phase methods based on hydrothermal, microwave, and other solvothermal approaches have been proposed for synthesizing Ga_2O_3.[30–37] However, such techniques generally require extended processing time of several days for acceptable synthesis yields.

The other material of interest for this work, that is, GaN, has become one of the main materials for the fabrication of optoelectronic devices, such as high-efficiency light-emitting diodes,[38–40] lasers,[41,42] photodetectors,[43] and solar cells,[44] due to its bulk wide bandgap ($E_g = 3.4$ eV).[45] This property is very profitable for optoelectronic applications.[46] For example, it has been theoretically predicted that 2D GaN monolayer can emit light in the deep ultraviolet range, indicating a potential application in sterilization and water purification.[47] However, traditional fabrication techniques, such as mechanical exfoliation, cannot be applied to produce 2D GaN due to the wurtzite structure of the GaN bulk, which holds covalent bonds in all three directions[48] (i.e., it is not a layered van dew Waals crystal as most group IV or transition metal dichalcogenides). Among all the fabrication techniques, chemical vapor deposition (CVD) and elemental epitaxial methods are the most common methods for the deposition of GaN thin films.[49–53] The epitaxial method is yet inherently limited by high cost, it does allow control of the formation of thin films, but only on carefully selected substrates. On the other hand, more affordable CVD methods cannot produce thin films with only a few unit-cell thicknesses, due to inherent nucleation limitations. Therefore, developing a substrate-independent, scalable process for synthesizing highly crystalline 2D GaN nanosheets across large areas would grant access to 2D GaN at a low cost.

Here, we propose a fast and low-cost synthesis approach for the growth of ultrathin Ga_2O_3, GaN, and gallium oxynitride (GaO_xN_y) layers, involving relatively low temperatures (<320 °C), which is fully compliant with the integration of 2D materials in photonic devices. This technique relies on a two-step process: the first step uses the 'liquid metal chemistry' (LMC) method, which has been recently developed[54,55] and proven effective for synthesizing large-scale ultrathin oxide and metallic layers with various compositions depending on the liquid metal precursor.[56] The second step involves a microwave plasma-enhanced nitridation reaction. The efficiency of LMC technique has been demonstrated for metals and metal alloys present in liquid form below ≈350 °C.[56] Using the LMC technique, we synthesize here ultrathin Ga_2O_3 nanosheets from the self-limiting oxide layer that forms on the surface of liquid gallium near room temperature in a few seconds. Next, our ultrathin Ga_2O_3 nanosheets undergo a microwave plasma-assisted nitridation reaction, eventually resulting in ultrathin GaN layers. We demonstrate, through X-ray photoelectron spectroscopy (XPS) measurements, that this two-step process grants us access to intermediate GaO_xN_y compounds, with tunable optical properties, ranging between those of Ga_2O_3 and GaN. This study also expands our knowledge on GaO_xN_y compounds, which have been scantily explored compared to their GaN and Ga_2O_3 counterparts.[57] Considering that Ga_2O_3 and GaN are widely used in luminescent and power devices, the characterization of their alloys fosters the development of materials with tailored properties and provides new opportunities to improve the device performance. We anticipate that this technique allows for the synthesis of ultrathin GaO_xN_y nanosheets that can be deposited directly onto flat substrates and silicon photonic devices with embedded optical waveguides. This technology thus paves the way toward the realization of hybrid photonic circuits that locally exploit 2D materials to adjust or enhance the optical properties of mature silicon photonic chips.

2. Fabrication of the Ultra-Thin Films and Nitridation Process

Our LMC-based synthesis relies on a two-step process, exploiting 1) the squeeze printing of liquid gallium, which results in ultrathin Ga_2O_3, and 2) its conversion into GaO_xN_y or GaN via a plasma-assisted nitridation treatment.

The growth process started by placing a droplet (≈1 mm in diameter) of liquid gallium (melting point. 29.8 °C) on an atomically flat centimeter-scale SiO_2/Si substrate. Following the Cabrera–Mott oxidation model depicted in **Figure 1**a, an ultrathin and self-limiting oxide layer formed on the liquid metal surface once it was exposed to the ambient atmosphere. Cabrera–Mott oxidation occured at the surface of liquid metals in the presence of oxygen at low/moderate temperatures. Electrons from the Ga metal tunneled through the growing oxide shell, resulting in a self-generated electric field called the Mott field.[54,56,58–64] This field promoted the diffusion of metal and oxygen ions into the oxide shell, leading to oxide growth. A glass slide was firmly pressed onto the droplet, effectively squeezing the droplet into the shape of a thin metal film. Upon removal of the top glass substrate, a large and continuous ultrathin gallium oxide film, which reached lateral dimensions exceeding several centimeters, remained on the SiO_2/Si sample. In order to remove the remaining liquid metal microdroplets, we used a solvent-assisted mechanical cleaning protocol based on ethanol heated to 75 °C. The SiO_2/Si sample with the deposited ultrathin Ga_2O_3 sheet was submerged in hot ethanol. Any metal inclusions can be entirely removed by wiping the SiO_2/Si wafer with a polyurethane foam swab while submerged, whereas the Ga_2O_3 sheet remained anchored on the substrate.[65]

Subsequently, our gallium oxide sheets were converted into gallium oxynitride or gallium nitride using a microwave-activated plasma reaction (Figure 1b). By controlling the plasma parameters (see methods), in particular the time and power, we can

© 2023 The Authors. Advanced Photonics Research published by Wiley-VCH GmbH

26999293, 0, Downloaded from https://onlinelibrary.wiley.com/doi/10.1002/adpr.202300252 by Readcube (Labtiva Inc.), Wiley Online Library on [20/12/2023]. See the Terms and Conditions (https://onlinelibrary.wiley.com/terms-and-conditions) on Wiley Online Library for rules of use; OA articles are governed by the applicable Creative Commons License

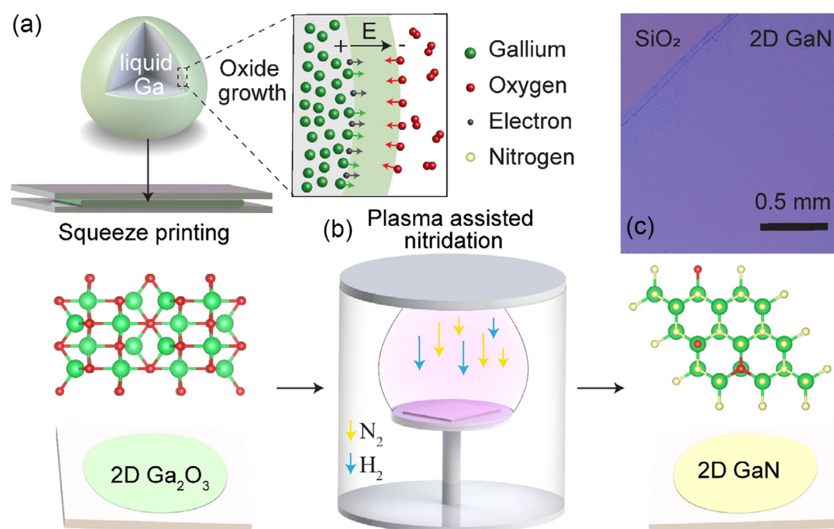

Figure 1. Synthesis process of large-area ultrathin GaN nanosheets. a) Schematic illustration of the Cabrera–Mott oxidation that occurs at the surface of liquid metals in the presence of oxygen followed by the printing technique used to exfoliate 2D oxides from molten metal. The liquid metal droplet is squeezed between two substrates allowing the transfer of the Ga_2O_3 layer. b) Synthesis process of the ultrathin GaN nanosheet from ultrathin layer of Ga_2O_3, utilizing a microwave-activated nitrogen/hydrogen plasma conducted in a cylindrical cavity plasma reactor. c) Optical image of the synthesized GaN on SiO_2/Si, confirming the presence of an ultrathin and homogeneous layer reaching several millimeters in lateral size.

either fully transform the oxide film into nitride or reach stabilized intermediate GaO_xN_y phases between Ga_2O_3 and GaN.

3. Results

3.1. X-ray Photoelectron Spectroscopy (XPS) of Ga_2O_3 and GaN Layers

To ascertain the quantitative conversion of Ga_2O_3 to GaN film, we analyzed the samples using XPS and we compared the relevant spectra before and after the nitridation process, using the plasma parameters indicated in the Experimental Section. **Figure 2**a,b shows the XPS spectra of a doublet in the Ga 2*p* region centered at ≈1118.19 and ≈1144.8 eV corresponding to $2p_{3/2}$ and $2p_{1/2}$, respectively, in good agreement with the spectral values for bulk and ultrathin Ga_2O_3 and GaN.[54,66,67] As anticipated, these signatures do not exhibit significant changes between Ga_2O_3 and GaN, with the two peaks observed at the same positions for both samples. Indeed, the electronic configuration of gallium remains similar in both compounds, with only the anion (oxygen or nitrogen) being replaced during the transformation process. As a result, the Ga 2*p* doublet peaks serve as a reliable marker for the presence of gallium in both Ga_2O_3 and GaN films. To distinguish between the two materials and investigate the extent of the conversion, we next compared the O 1*s* peak for Ga_2O_3 and GaN (i.e., before and after the nitridation process). In Figure 2c (Ga_2O_3), we can see a double peak for O 1*s*: the peak at ≈530.9 eV can be assigned to the O—Ga—O bonds in gallium oxide, and the O 1*s* peak at binding energy ≈532.2 eV can be ascribed to the Si—O bonding from the SiO_2 substrate layer underneath.[68] In contrast, after the nitridation process, only one single O 1*s* peak is detected on Figure 2d, centered at ≈532.2 eV. The disappearance of the shorter energy peak thus confirms the effectiveness of the nitridation process for fully converting Ga_2O_3 into GaN. (See Figure S1, Supporting Information).

3.2. Tailoring the GaO_xN_y Composition via Plasma-Assisted Nitridation

The presence of residual oxygen can significantly affect the structural, electrical, and optical properties of the material. In this context, during the nitridation process, a careful control of the plasma conditions, such as power, pressure, and gas flow, enables us to tailor the amount of the oxygen substitution. In order to explore how the oxygen substitution can be controlled, the nitridation process was conducted under various powers and time duration. First, the plasma was generated for 10 min at different powers of 100, 150, and 200 W. As displayed in **Figure 3**a, XPS results show that by increasing the power, the atomic percentage of oxygen in the sample decreases, while the percentage of nitrogen increases, demonstrating a more effective replacement of oxygen with nitrogen bonds to gallium. By increasing the power to 200 W, the complete removal of oxygen was achieved. Alternatively, Figure 3b presents the XPS results of five samples with different nitridation times varying from 0 to 10 min. During this experiment, power was kept constant at 150 W. Over time, as plasma exposure continues, the Ga_2O_3 film is gradually converted to GaN. This evidence is proved by the atomic ratios measured through XPS, showing a decrease in the oxygen percentage to gallium bond from 57.2 to 2.5 at% and an increase in the rate of nitrogen bonds to gallium from 0 to 46.5 at%. (See Experimental Section).This confirms that the control of either the power and/or time duration of the plasma-assisted nitridation process allows us to reliably obtain intermediate compositions of GaO_xN_y films.

© 2023 The Authors. Advanced Photonics Research published by Wiley-VCH GmbH

26999293, 0, Downloaded from https://onlinelibrary.wiley.com/doi/10.1002/adpr.202300252 by Readcube (Labtiva Inc.), Wiley Online Library on [20/12/2023]. See the Terms and Conditions (https://onlinelibrary.wiley.com/terms-and-conditions) on Wiley Online Library for rules of use; OA articles are governed by the applicable Creative Commons License

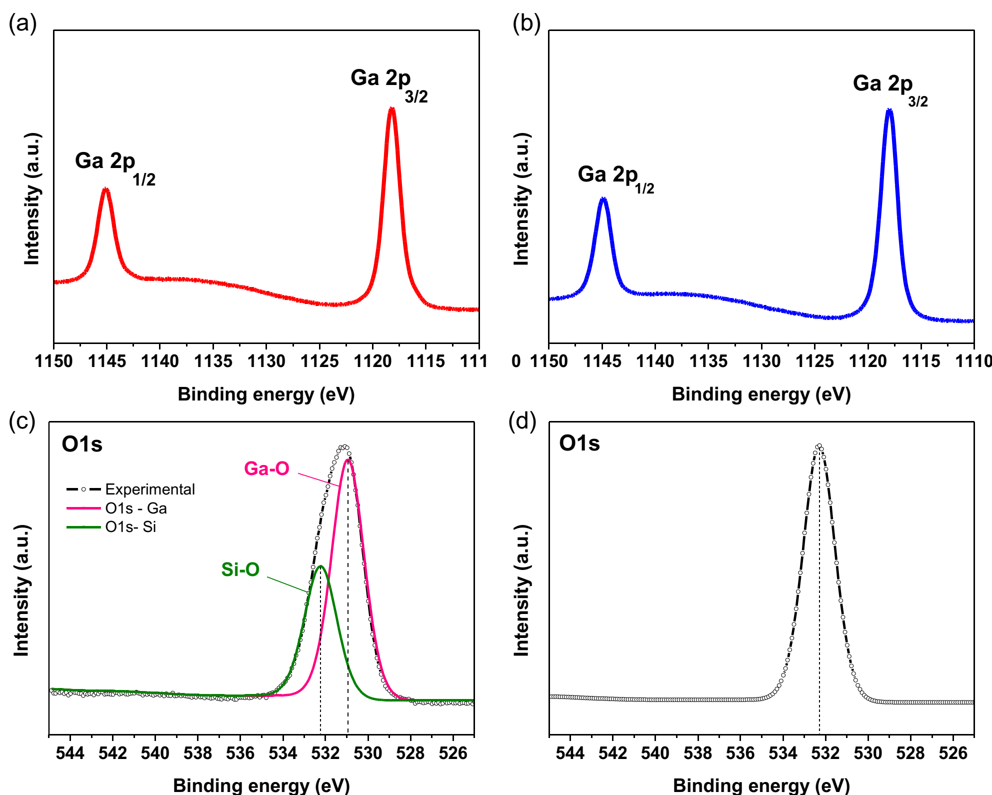

Figure 2. Material characterization of ultrathin Ga_2O_3 (before nitridation (a and c)) and ultrathin GaN (after the nitridation (b and d)) on a SiO_2/Si substrate. a,c) XPS results of the ultrathin Ga_2O_3 for the spectral regions of interest, around (a) the Ga 2*p* peak and (c) the O 1*s* peak. b,d) XPS result for the the ultrathin GaN around (b) the Ga 2*p* peak and (d) the O 1*s* peak.

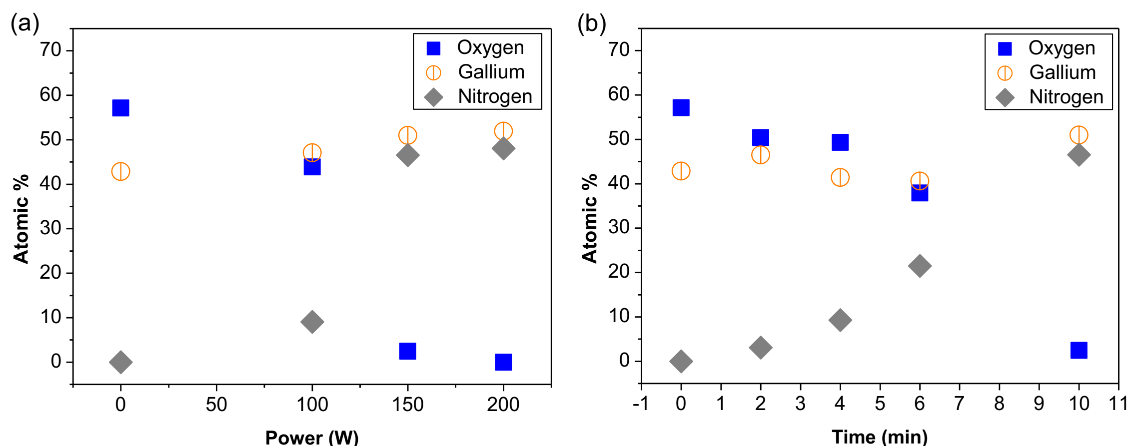

Figure 3. XPS data for Ga_2O_3/SiO_2/Si samples that have undergone a plasma nitridation reaction with a) a varying power (constant time = 10 min) or b) a variable plasma duration (constant power = 150 W).

3.3. AFM and TEM Structural Characterization of the GaN and Ga_2O_3 Layers

The uniformity of the synthesized ultrathin GaN sheets was checked through atomic force microscopy (AFM) on the deposited layer. **Figure 4**a shows the results from the measurement. After the full nitridation process, GaN formed a continuous and atomically flat nanosheet, $\approx 3 \pm 0.2$ nm in thickness. This thickness was found to be similar to that of the initial Ga_2O_3, showing that the nitridation does not affect the thickness of the film. In general, the ultrathin sheets feature minimal cracks and holes, and a relatively homogeneous thickness across large distances, which is compatible with the typical size of integrated optical devices as sought for optoelectronic application prospects.

© 2023 The Authors. Advanced Photonics Research published by Wiley-VCH GmbH

26999293, 0, Downloaded from https://onlinelibrary.wiley.com/doi/10.1002/adpr.202300252 by Readcube (Labtiva Inc.), Wiley Online Library on [20/12/2023]. See the Terms and Conditions (https://onlinelibrary.wiley.com/terms-and-conditions) on Wiley Online Library for rules of use; OA articles are governed by the applicable Creative Commons License

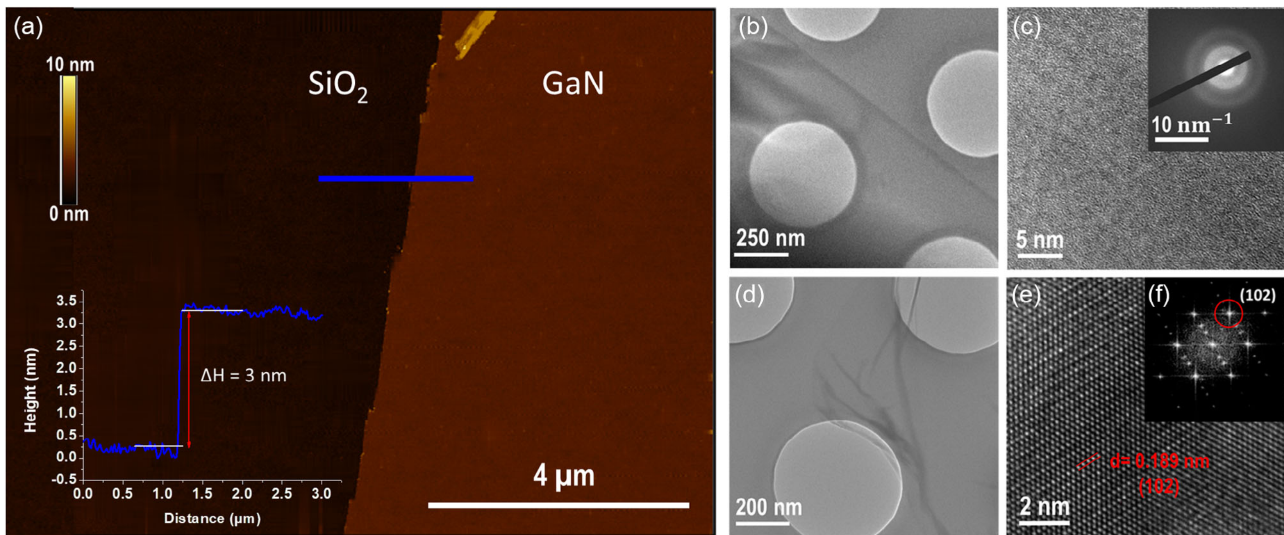

Figure 4. Morphology and structural characterization of ultrathin Ga_2O_3 and GaN. a) AFM topography image of a GaN sample taken at the edge of a nanosheet; the height profile was measured along the blue line. b–e) Structural characterization of the ultrathin film before and after full nitridation, (b) TEM micrograph of the Ga_2O_3, (c) Ga_2O_3 lattice fringe and the corresponding SAED pattern, (d) HRTEM micrograph of the GaN, (e) insets representing the lattice fringes of GaN. f) Fast Fourier transform pattern demonstrating (102) plane of the GaN sheet.

Transmission electron microscopy (TEM) and high-resolution TEM (HRTEM) were utilized to further characterize the morphology and assess the crystallographic properties of the gallium sheets before and after nitridation. Gallium oxide was directly deposited onto a Si_3N_4 TEM grid (Figure 4b). Figure 4c shows that no crystalline structure is visible in the TEM maps of the ultrathin Ga_2O_3, confirming that the latter has an amorphous structure. The combination of low temperature and rapid growth kinetics during the squeeze printing method leads to the formation of amorphous Ga_2O_3 structures within seconds. Annealing of the obtained Ga_2O_3 at 370 °C is shown to have negligible effects on its crystalline properties in which Ga_2O_3 remains amorphous when exposed to these temperatures.[69] However, in this work, the Ga_2O_3 deposited on Si_3N_4 TEM grid was converted to GaN using the same plasma treatment (utilizing a mixed gas plasma of H_2 and N_2, we operate at 320 °C). It is worth noting that plasma-assisted synthesis is known to yield crystalline GaN at approximately this temperature.[70] Ultrathin nanosheets can now be found during TEM imaging, with the sheets being highly translucent, indicating the thin nature of the final GaN sample (Figure 4d–f). HRTEM confirmed the crystalline nature of the GaN samples with a lattice spacing of ≈0.189 nm, corresponding to the (102) planes of wurtzite phases.

3.4. Ellipsometry Characterization of the Ultrathin GaN, Ga_2O_3, and GaO_xN_y Layers

The knowledge of the Ga_2O_3 and GaN refractive index is essential to properly design gallium-based optoelectronic devices. Although the optical properties of Ga_2O_3 thin films (down to sev. 10's of nm) have been investigated,[71–74] there remains a lack of experimental measurements of the properties of ultrathin Ga_2O_3 sheets with a few nanometers thickness. Similarly, for GaN, the available data focus on either bulk or thin layers

Table 1. Comparison of refractive index measurement for Ga_2O_3 and GaN at different thicknesses.

Material	Thickness	n	λ [nm]	References
Ga_2O_3	Bulk	1.84–1.88	980	[107]
Ga_2O_3	67.9 nm	1.84	632	[92]
Ga_2O_3	31.9–2468 nm	1.89	295–826	[108]
Ga_2O_3	30 nm	1.87	632	[84]
Ga_2O_3	89 nm	1.85	632	[109]
Ga_2O_3	**3 nm**	**1.89**	**632**	**This work**
GaN	Bulk	2.34	632	[110]
GaN	2.3 μm	2.42	632	[87]
GaN	1.5 μm	2.33	632	[79]
GaN	1.3 μm	2.37	632	[78]
GaN	1.06 μm	2.34	632	[88]
GaN	532 nm	2.1	1200	[89]
GaN	**3 nm**	**2.31**	**632**	**This work**

(mentioned in **Table 1**) and are not directly applicable to ultrathin (≈3 nm) GaN sheets.[75–79] Therefore, the properties of both materials in their 2D form remain elusive. Spectroscopic ellipsometry (SE) has been used to study bulk optical properties of Ga_2O_3[80–84] and Ga[8,85–89] In recent years, SE has emerged as a valuable tool also for investigating the optical properties of 2D materials.[90,91] Here, we characterized the Ga_2O_3 and GaN ultrathin films as well as GaO_xN_y intermediate compounds with SE. The substrate used for all the ultrathin films was SiO_2/Si with a 3 nm-thick silica layer. The optical indices of Ga_2O_3 and GaN were determined by fitting the I_s and I_c parameters of the SE data measured before or after the full nitridation process. For both cases, the dispersion of the 3 nm-thick layer was accounted

© 2023 The Authors. Advanced Photonics Research published by Wiley-VCH GmbH

26999293, 0, Downloaded from https://onlinelibrary.wiley.com/doi/10.1002/adpr.202300252 by Readcube (Labtiva Inc.), Wiley Online Library on [20/12/2023]. See the Terms and Conditions (https://onlinelibrary.wiley.com/terms-and-conditions) on Wiley Online Library for rules of use; OA articles are governed by the applicable Creative Commons License

26999293, 0, Downloaded from https://onlinelibrary.wiley.com/doi/10.1002/adpr.202300252 by Readcube (Labtiva Inc.), Wiley Online Library on [20/12/2023]. See the Terms and Conditions (https://onlinelibrary.wiley.com/terms-and-conditions) on Wiley Online Library for rules of use; OA articles are governed by the applicable Creative Commons License

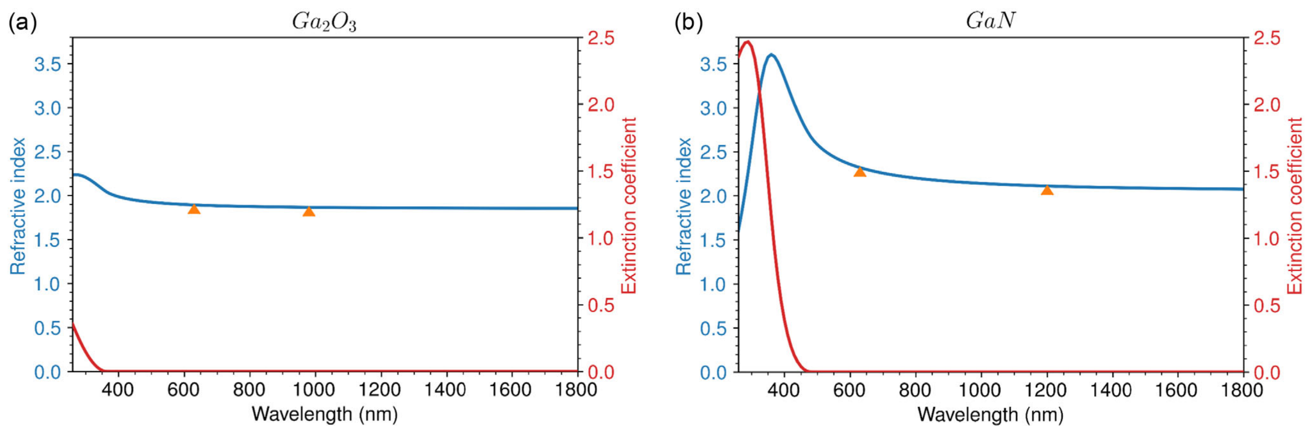

Figure 5. Optical properties of Ga_2O_3 and GaN ultra-thin films, extracted from SE in the range 260–1800 nm. a) Refractive index n and extinction coefficient k of Ga_2O_3 as a function of wavelength (triangles shows $n = 1.89$ at 632 nm and $n = 1.865$ at 980 nm). b) Refractive index n and extinction coefficient k of GaN as a function of wavelength (triangles shows $n = 2.318$ at 632 nm and $n = 2.1$ at 1200 nm).

for by a Tauc–Lorentz formula with adjusted parameters. The model also included the 3 nm-thick SiO_2 native oxide of the SiO_2/ Si host substrate.

Figure 5a shows the refractive index (n) and the extinction coefficient (k) of the Ga_2O_3 layer. The resulting refractive index is found to be 1.89 at 632 nm and 1.865 at 980 nm wavelength. Despite the reduced thickness of our films (≈3 nm), these values are very close to those measured for Ga_2O_3 68 nm-thick films ($n = 1.84$ at 632 nm),[92] or Ga_2O_3 800 nm-thick films ($n = 1.82$ at 600 nm).[93]

Figure 5b displays the n and k spectra of GaN measured after the full nitridation process. The extracted refractive index was changed to 2.318 at 632 nm and 2.1 at 1200 nm, showing that the nitridation process was effective in turning the oxide films into GaN with distinct optical properties. Again, this refractive index value is only slightly lower than the values found in the literature for bulk GaN crystals ($n = 2.34$ at 632 nm), metal–organic chemical vapor-deposited GaN layers ($\underline{n} = 2.33$ at 632 nm) on sapphire from another study,[85] and GaN epilayers ($n \approx 2.42$ at 632 nm) from another study[87] Moreover, the refractive index at 1200 nm is consistent with another study[89] for GaN films with 532 nm thickness. A summary of the comparison of our work and the literature on Ga_2O_3 and GaN measured refractive index (n) at different thicknesses and wavelengths (λ) is reported in

Table 1 Considering that our measured value for 3 nm-thick films is in the same range as for bulk and thick films, we conclude that the refractive index of these materials remains roughly constant regardless of changes in film thickness. In addition, by comparing the refractive index of Ga_2O_3 and GaN at the same wavelength, we note that the relatively high-index difference (≈0.42), featuring a significant ≈20% variation could be relevant for adjusting the optical properties of silicon photonic devices on top of which this ultrathin material is deposited.

In order to measure the effective index of the intermediate GaO_xN_y layers, the related ellipsometry spectra were fit using an effective medium model (Bruggeman). This model considers that the layer on top of the SiO_2/Si substrate consists of a composite (mixed) GaN/Ga_2O_3 layer, with each material following the Tauc–Lorentz dispersion formula extracted from the previous measurements (i.e., for the GaN and Ga_2O_3 layer). For these intermediate GaO_xN_y compounds, only the percentage ratio of GaN to Ga_2O_3 in the mixed layer is used to fit the data, while the thickness (3 nm) and the corresponding dispersion relation for either the GaN to Ga_2O_3 layer were kept fixed, in accordance with the results of

Figure 5 This model allows us to extract the effective refractive index, extinction coefficient of the GaO_xN_y layer, as well as the "ratio" of GaN in the modeled composite layer. **Figure 6**a,b shows the measurement of the effective index of the intermediate GaO_xN_y compounds. Panel a (panel b) presents the evolution of n and k as the plasma power (or time duration) is increased. The evident variations observed on these curves strongly depend on the degree of nitridation of the oxide film. These results indicate that the optical properties of the ultrathin GaO_xN_y film can be reliably adjusted by the plasma parameters in a controlled manner, as would be useful for photonic device applications. Figure 6c,d shows the increase of refractive index at 1550 nm wavelength as a function of the plasma power and time adopted during the plasma nitridation treatment, respectively. These data show an increase of the fitted percentage of GaN in the modeled layer as a function of the plasma parameters, which is consistent with the XPS measurements in Figure 3. This re-emphasizes the effectiveness of the plasma treatment to turn the oxide layer into GaN in a gradual and controlled manner.

3.5. DFT Calculation

First-principles simulations were carried out to corroborate the optical properties of GaN and Ga_2O_3 and to unravel the effect of crystallinity and atomic disorder on the optical response of those materials.The theoretical calculations were performed within the framework of density functional theory (DFT) as implemented in the Quantum Espresso (QE) package (see Experimental Section).[94] In order to get rid the statistical complexity of dealing with amorphous systems, in this work, we considered the electronic and optical properties only of Ga_2O_3 crystal in the monoclinic phase. Even though this may appear as a too crude

 © 2023 The Authors. Advanced Photonics Research published by Wiley-VCH GmbH

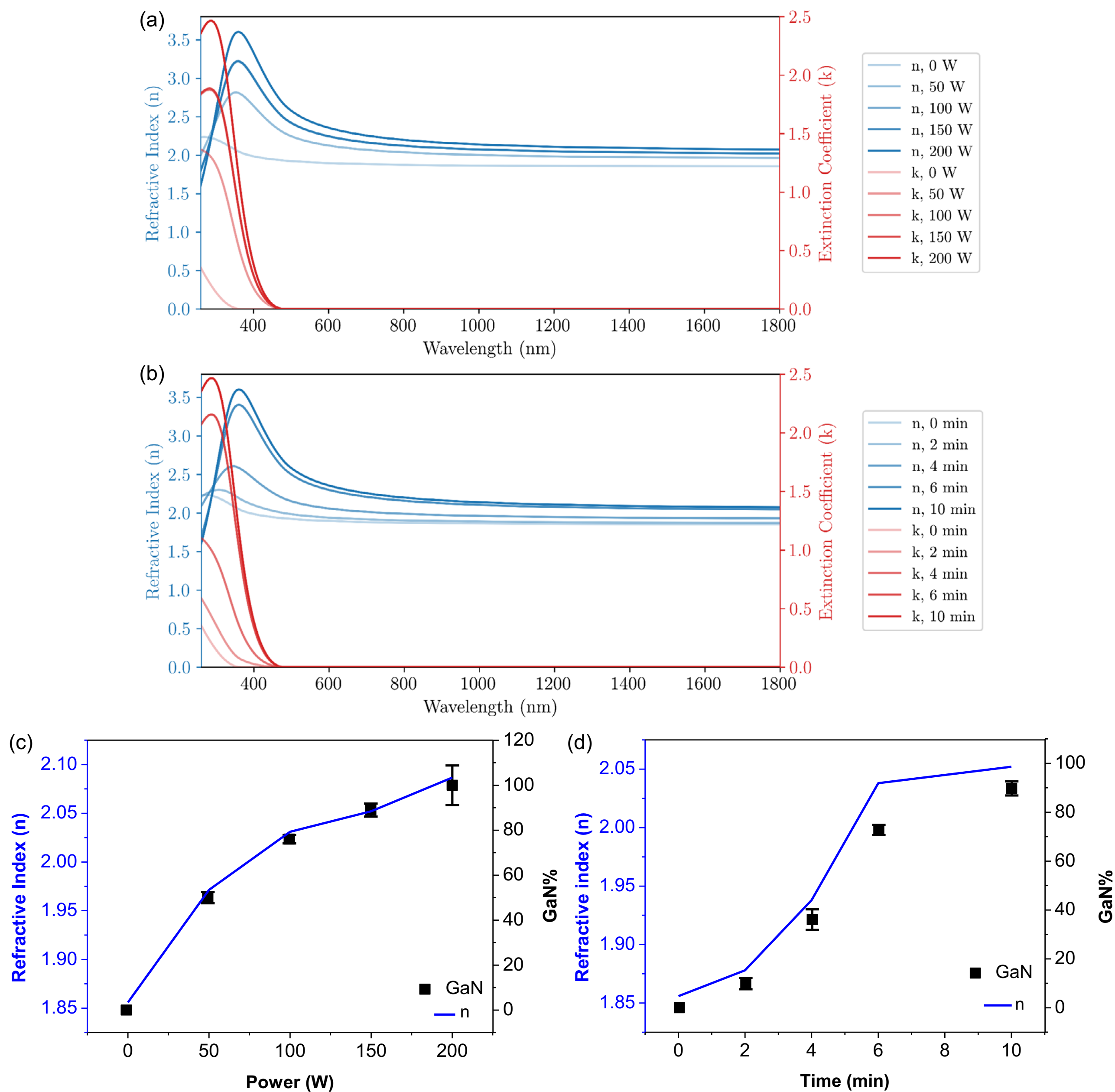

Figure 6. a,b) Optical properties of the oxynitride ultrathin films, extracted from SE in the range 260–2100 nm. (a) The variation of refractive index n and extinction coefficient k of GaO_xN_y as a function of wavelength upon increasing the plasma power. (b) Variation of refractive index n and extinction coefficient k of GaO_xN_y as a function of wavelength upon increasing the plasma time duration. c) Increase in GaN percentage (black squares) and refractive index (blue line), extracted from ellipsometry as a function of power (constant time = 10 min). d) Increase in GaN percentage (back squares) and refractive index (blue line), extracted from ellipsometry as a function of time (constant power = 150 W).

approximation, this choice is justified by the well-known observation that the polar nature of the bonds in metal oxides (with respect, e.g., to the covalent character of Si or Ge) makes the system almost insensitive to structural distortions.[95,96] As a consequence, the optical properties of most amorphous oxides are very similar to their crystalline counterpart.

Figure 7 shows the bulk unit cells of Ga_2O_3 (panel a) and GaN (panel b) that were considered in the calculations. The optimized lattice parameters for monoclinic β-Ga_2O_3 crystal are $a = 12.42$ Å, $b = 3.08$ Å and $c = 5.87$ Å, and $b = 103.74°$, while those for the wurtzite GaN are $a = b = 3.22$ Å and $c = 5.24$ Å, in good agreement with previous DFT calculations.[97,98]

© 2023 The Authors. Advanced Photonics Research published by Wiley-VCH GmbH

26999293, 0, Downloaded from https://onlinelibrary.wiley.com/doi/10.1002/adpr.202300252 by Readcube (Labtiva Inc.), Wiley Online Library on [20/12/2023]. See the Terms and Conditions (https://onlinelibrary.wiley.com/terms-and-conditions) on Wiley Online Library for rules of use; OA articles are governed by the applicable Creative Commons License

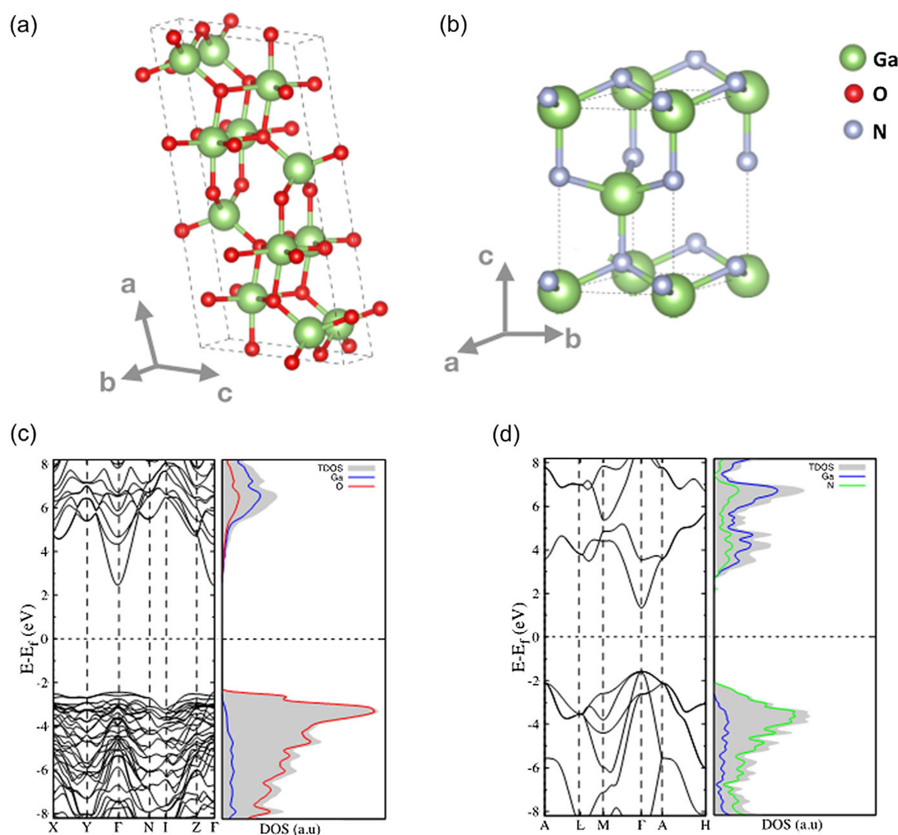

Figure 7. Atomic structure of a) β-Ga_2O_3 and b) GaN bulk crystals. Bandstructure (left panels) and the total and atom projected DOS (right panels) of c) β-Ga_2O_3 and d) GaN, respectively. Zero energy reference is set to the Fermi level (E_f) of each system.

The density of states (DOS) and band structure of β-Ga_2O_3 and GaN are shown in Figure 7c,d, respectively. The well-known underestimation of the bandgap (E_g) due to the standard DFT functionals has been corrected by including a Hubbard-like potential on each chemical species, within the DFT + U frameworks.[99] Both materials have a direct bandgap, namely, $E_g = 2.93$ for GaN and $E_g = 4.89$ eV for β-Ga_2O_3. The calculated values are very close to those calculated at Heyd-Scuseria-Ernzerhof (HSE) level, and in very good agreement with experimental data, confirming the numerical accuracy of the methodology used in our calculations.[100] The projected DOS plots indicate that in both cases the top of the valence band has mainly a nonmetal, that is, O, N, character, with a small contribution from Ga *sp*-orbitals. The bottom of the conduction band has an almost equal contribution of O (N) and Ga orbitals. The different polarity of the Ga—O and Ga—N bonds is mainly

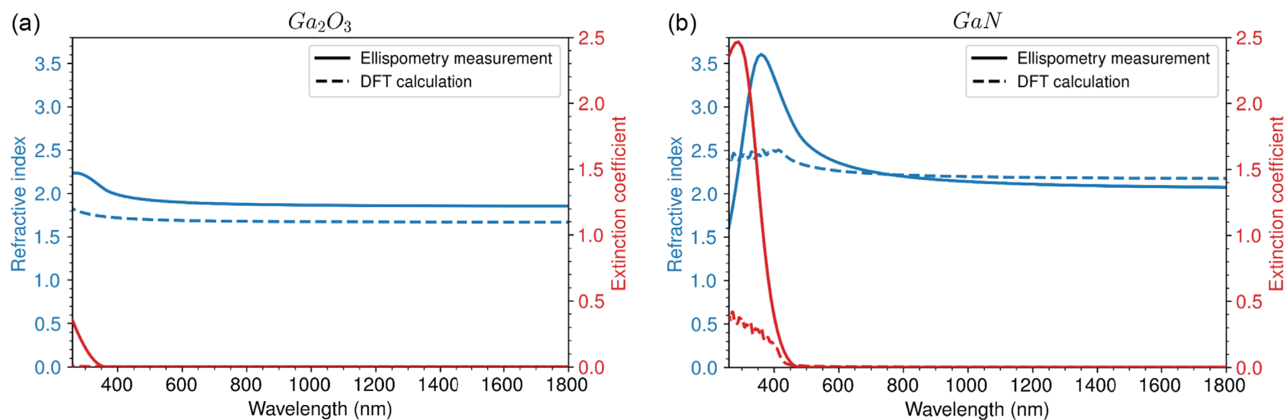

Figure 8. Optical properties of Ga_2O_3 and GaN ultrathin films, extracted from DFT in the range 260–1800 nm. a) The refractive index *n* and extinction coefficient *k* of Ga_2O_3 as a function of wavelength. b) The refractive index *n* and extinction coefficient *k* of GaN as a function of wavelength.

© 2023 The Authors. Advanced Photonics Research published by Wiley-VCH GmbH

26999293, 0, Downloaded from https://onlinelibrary.wiley.com/doi/10.1002/adpr.202300252 by Readcube (Labtiva Inc.), Wiley Online Library on [20/12/2023]. See the Terms and Conditions (https://onlinelibrary.wiley.com/terms-and-conditions) on Wiley Online Library for rules of use; OA articles are governed by the applicable Creative Commons License

responsible for the different bandgaps and thus of the different optical properties. Further localized states close to the mobility gap might appear in the amorphous structure of Ga_2O_3.[101] This does not change the overall scenario described below about the optical response of the metal-oxide system.

Figure 8 shows the refractive indices and extinction coefficients spectra of Ga_2O_3 (panel a) and GaN (panel b) nanolayers obtained from the SE experiments compared with the DFT results of the corresponding bulk crystals. The theoretical absorption edge is at $\lambda = 253$ nm ($\lambda = 423$ nm) for Ga_2O_3 (GaN), respectively, which corresponds to the valence-to-conduction bandgap. Despite the numerical differences (mostly probably related to the effect of the residual presence of defects and impurities), the agreement between the experimental and DFT optical indices brings two important conclusions: 1) the experimental data for GaN well fit the results for crystalline (i.e., ordered) phase. This corroborates the analysis related to the structural quality of the ultrathin layer and the effectiveness of the nitridation process. The good agreement observed also in the Ga_2O_3 case confirms a posteriori our initial choice of considering the monoclinic crystal structure, instead of the experimental amorphous one. 2) The experimental data for nanosheets well fit the results for extended bulk (i.e., extended) materials. This confirms the observation that ultrathin films fast recover the bulk/thick film properties, getting rid of strong localization and or major surface effects.

4. Conclusion

We reported the synthesis of ultrathin (≈3 nm thick) GaO_xN_y films, with an adjusted composition between that of Ga_2O_3 and GaN, using an easy and low-cost two-step process, relying on the liquid metal-based van der Waals squeeze printing technique followed by a plasma-assisted nitridation process. XPS analysis indicates that the use of a reactive N_2/H_2 plasma in the latter step is key to obtain an ultrathin GaN layer from replacing oxygen atoms with nitrogen ones in the squeeze-printed Ga_2O_3 film. Furthermore, we showed that, through adjusting plasma power and exposure time of the nitridation process, we could achieve tailored compositions of the GaO_xN_y ultrathin layers, with intermediate optical properties between those of Ga_2O_3 and GaN. We characterized the composition and optical properties of the resulting nanometer-thick Ga_2O_3, GaN, and GaO_xN_y ultrathin films. DFT calculations of Ga_2O_3 and GaN were conducted to compare the optical indices obtained by ellipsometry and give further evidence of the nature of the resulting thin films. The comparison between the optical index measurement conducted on these ultrathin films and those extracted from the literature shows that the refractive index of these ultrathin Ga_2O_3 and GaN materials does not depend much on the film thickness, at least down to 3 nm, as was investigated here.

The proposed synthesis method is scalable and fast, as well as compatible with low-temperature (<320 °C) processes, granting the access to large-area ulrathin Ga_2O_3 and GaN nanosheets. This offers new opportunities for the direct deposition of these ultrathin films onto chip-based photonic devices. The measurement of the effective index of the GaO_xN_y ultrathin film across the visible and near-IR range shows that a significant and controlled 20% variation of the ultrathin film refractive index can be achieved by tuning the composition. This can be exploited for adjusting the properties of optical devices based on these materials. In the longer term, this work provides a pathway toward the integration of 2D materials to create efficient hybrid photonic chips and locally adjust or functionalize an otherwise passive optical circuit.

5. Experimental Section

Transformation of 2D Ga_2O_3 to 2D GaN Sheets via Microwave Plasma-Assisted Nitridation Process: This transformation was afforded by a commercially available Plasma-Therm Vision 310 plasma-enhanced chemical vapor deposition (PECVD) equipment. The synthesis was carried out in a microwave plasma-enhanced CVD reactor at a substrate temperature of ≈320 °C using a plasma consisting of N_2 (99.5%) and H_2 (0.5%). The pressure in the plasma chamber was 1 Torr. The plasma was generated with radio frequency power of 150 W, while the concentration of the H_2/N_2 gas mixture was controlled by setting flow rate of the gases to 200 sccm/1 sccm, respectively. A small amount of H_2 plasma was used to improve the nitridation process by reducing the oxide of the nanosheets. During the transformation to GaN, the samples were exposed to the plasma for 10 min. While this specific plasma treatment recipe led to a full conversion of the oxide film into nitride, a slight change in the plasma power and time duration enabled us to reach intermediate GaO_xN_y phases between Ga_2O_3 and GaN.

Material Characterization: XPS analysis was conducted on materials grown on SiO_2/Si substrates using a Thermo Scientific K-alpha XPS spectrometer equipped with a monochromatic Al Kα source ($h\nu = \approx 1486.7$ eV). The analyzer was operated with a pass energy of 50 eV to record the core-level spectra from a 300 μm spot size and 50 number of scans for each sample. A low-energy electron flood gun was utilized to remove the surface charging effect of the synthesized material without an ion gun. All the elements were adjusted with the C—C bond of carbon at 284.68 eV.All peaks were fit using Thermo Scientific Advantage Software V5.9. The scanned areas were automatically calculated using the Advantage software V5.9 to verify the atomic ratios and compositions. AFM image was obtained using a Park NX10 AFM. Gwyddion 2.56 software was utilized for AFM image processing and analysis. The high-resolution TEM measurements were performed using a JEOL JEM-F200 TEM with acceleration voltages of 200 kV. The Gatan micrograph 3.4. Software Package was used for TEM/HRTEM analysis. Thermally and mechanically robust Si3N4 TEM (Ted Pella, 21 587-10) membranes were used to develop the TEM samples that were prepared by directly printing the gallium oxide sheet onto TEM membrane and subsequent PECVD. The Si3N4 TEM grid allows experiments requiring temperatures up to 1000 °C, which suits the synthesis process presented in this work. The Si3N4 TEM grids also featured pores which were completely empty and allowed analysis of the suspended flakes through the pore without contribution of the TEM grid. The ellipsometric characterization was performed using a Jobin Yvon-UVISEL spectroscopic, covering a wavelength range from 260 to 2100 nm at 70° of incidence angle.

DFT Calculation: The theoretical calculations were performed within the framework of DFT as implemented in QE package. The exchange-correlation term was described by generalized gradient approximation –Perdew–Burke–Ernzerhof functional.[102] The electron−ion interactions were treated within the optimized norm-conserving Vanderbilt pseudopotentials and the energy cutoff was fixed at 95 Ry for expanding the plane-waves.[103] A Γ-point-centered Monkhorst–Pack mesh of $13 \times 11 \times 1$ grid was used to perform the integration over Brillouin zone with a Marzari–Vanderbilt smearing of 0.15 eV. All atomic positions were allowed to relax until the forces acting on each atom were less than 0.02 eV Å^{-1} and the convergence threshold of the energy change was set at 10^{-5} eV.

Undesired DFT bandgap underestimation was corrected by including system-tailored Hubbard-like correction to each atomic species. The adopted values resulted from the self-consistent pseudo-hybrid Hubbard density functional approach implemented in the ACBN0 approach.[104] In the case of wurtzite GaN, the optimized values were $U_{3d}(\mathrm{Ga})^{\mathrm{GaN}} = 19.18$ eV

© 2023 The Authors. Advanced Photonics Research published by Wiley-VCH GmbH

26999293, 0, Downloaded from https://onlinelibrary.wiley.com/doi/10.1002/adpr.202300252 by Readcube (Labtiva Inc.), Wiley Online Library on [20/12/2023]. See the Terms and Conditions (https://onlinelibrary.wiley.com/terms-and-conditions) on Wiley Online Library for rules of use; OA articles are governed by the applicable Creative Commons License

and $U_{2p}(N) = 3.92$ eV. The unitary cell of monocliclic Ga_2O_3 included two set of inequivalent Ga and O atoms. The corresponding U values were $U_{3d}(Ga_1)^{Ga2O3} = 17.85$ eV, $U_{3d}(Ga_2)^{Ga2O3} = 18.08$ eV, $U_{2p}(O_1) = 7.89$ eV, and $U_{2p}(O_2) = 8.10$ eV. Further accuracy tests on the effects of the inclusion of Hubbard-like correction on the bandgap as well as the dielectric and vibrational properties of semiconductors can be found in other studies.[104–106]

The optical properties were evaluated from first principles, using the ε_x code, contained in the QE package. The code implements a band-to-band single-particle approach based on a generalized Drude–Lorentz formulation of the macroscopic dielectric function $\hat{\varepsilon} = \varepsilon_1 + i\varepsilon_2$.[106] The refractive index (n) and extinction coefficient (k) were straightforwardly obtained from the algebraic transformation of the real (ε_1) and the imaginary (ε_2) part of the dielectric function: $n = \{1/2[(\varepsilon_1^2 + \varepsilon_2^2)^{1/2} + \varepsilon_1]\}^{1/2}$, $k = \{1/2[(\varepsilon_1^2 + \varepsilon_2^2)^{1/2} - \varepsilon_1]\}^{1/2}$.

Supporting Information

Supporting Information is available from the Wiley Online Library or from the author.

Acknowledgements

The authors thank the facilities and technical assistance of the Institute Nanotechnology De Lyon (INL) and RMIT Micro Nano Research Facility (MNRF) and the assistance of RMIT Microscopy and Microanalysis Facility (RMMF). The authors also thank The I3E ECLAUSion project that supported this project under funding from the European Union's Horizon 2020 research and innovation program under the Marie Skłodowska-Curie grant agreement no 801512 and ALphFA. The authors also acknowledge TD and KCN funding received from the Australian research council via the DECRA program (DE190100100).

Conflict of Interest

The authors declare no conflict of interest.

Data Availability Statement

The data that support the findings of this study are available from the corresponding author upon reasonable request.

Keywords

2D materials, gallium nitride, gallium oxide, liquid metal chemistry

Received: September 6, 2023
Revised: November 21, 2023
Published online:

[1] N. Mounet, M. Gibertini, P. Schwaller, D. Campi, A. Merkys, A. Marrazzo, T. Sohier, I. E. Castelli, A. Cepellotti, G. Pizzi, N. Marzari, *Nat. Nanotechnol.* **2018**, *13*, 246.
[2] J. Cheng, C. Wang, X. Zou, L. Liao, *Adv. Opt. Mater.* **2019**, *7*, 1800441.
[3] K. S. Novoselov, *Science* **2004**, *306*, 341.
[4] P. Miró, M. Audiffred, T. Heine, *Chem. Soc. Rev.* **2014**, *43*, 6537.
[5] D. Akinwande, C. J. Brennan, J. S. Bunch, P. Egberts, J. R. Felts, H. Gao, R. Huang, J. S. Kim, T. Li, Y. Li, K. M. Liechti, N. Lu, H. S. Park, E. J. Reed, P. Wang, B. I. Yakobson, T. Zhang, Y. W. Zhang, Y. Zhou, Y. Zhu, *Extreme Mech. Lett.* **2017**, *13*, 42.
[6] S. Z. Butler, S. M. Hollen, L. Cao, Y. Cui, J. A. Gupta, H. R. Gutiérrez, T. F. Heinz, S. S. Hong, J. Huang, A. F. Ismach, E. Johnston-Halperin, M. Kuno, V. V. Plashnitsa, R. D. Robinson, R. S. Ruoff, S. Salahuddin, J. Shan, L. Shi, M. G. Spencer, M. Terrones, W. Windl, J. E. Goldberger, *ACS Nano* **2013**, *7*, 2898.
[7] P. Sun, K. Wang, H. Zhu, *Adv. Mater.* **2016**, *28*, 2287.
[8] T. J. Kim, J. S. Byun, Y. D. Kim, Y. C. Chang, H. J. Kim, *J. Korean Phys. Soc.* **2008**, *53*, 1575.
[9] Y. Wei, R. Yang, *Natl. Sci. Rev.* **2019**, *6*, 324.
[10] A. Splendiani, L. Sun, Y. Zhang, T. Li, J. Kim, C. Y. Chim, G. Galli, F. Wang, *Nano Lett.* **2010**, *10*, 1271.
[11] K. S. Novoselov, A. Mishchenko, A. Carvalho, A. H. Castro Neto, *Science* **2016**, *353*, aac9439.
[12] D. Deng, K. S. Novoselov, Q. Fu, N. Zheng, Z. Tian, X. Bao, *Nat. Nanotechnol.* **2016**, *11*, 218.
[13] F. Xia, H. Wang, D. Xiao, M. Dubey, A. Ramasubramaniam, *Nat. Photonics* **2014**, *8*, 899.
[14] C. H. Liu, Y. C. Chang, T. B. Norris, Z. Zhong, *Nat. Nanotechnol.* **2014**, *9*, 273.
[15] J. Guo, J. Li, C. Liu, Y. Yin, W. Wang, Z. Ni, Z. Fu, H. Yu, Y. Xu, Y. Shi, Y. Ma, S. Gao, L. Tong, D. Dai, *Light: Sci. Appl.* **2020**, *9*, 29.
[16] D. K. Sarfo, R. R. Taylor, A. P. O. Mullane, *ACS Appl. Electron. Mater.* **2020**, *2*, 2921.
[17] B. R. Tak, S. Kumar, A. K. Kapoor, D. Wang, X. Li, *J. Phys. D: Appl. Phys.* **2021**, *54*, 453002.
[18] M. Kim, S. Seo, *Mol. Cryst. Liq. Cryst.* **2019**, *685*, 40.
[19] M. Mas-torrent, *ACS Appl. Electron. Mater.* **2020**, *2*, 3093.
[20] Y.G. Park, Y. G. Lee, J. Jang, S. M. Yun, E. Kim, J. U. Park, *Adv. Healthc. Mater.* **2021**, *10*, 2002280.
[21] M. B. Ghasemian, F. Allioux, S. Cai, P. Koshy, N. Gaston, K. Kalantar-zadeh, *Science* **2022**, *1124*, 1118.
[22] M. Mayyas, M. Mousavi, M. B. Ghasemian, R. Abbasi, H. Li, M. J. Christoe, J. Han, Y. Wang, C. Zhang, A. Rahim, J. Tang, J. Yang, D. Esra, R. Jalili, F. Allioux, A. P. O. Mullane, K. Kalantar-zadeh, *ACS Nano* **2020**, *14*, 14070.
[23] M. Karbalaei, F. Verpoort, S. Zhuiykov, *Appl. Mater. Today* **2022**, *27*, 101461.
[24] R. Binions, C. J. Carmalt, I. P. Parkin, K. F. E. Pratt, G. A. Shaw, *Chem. Mater.* **2004**, *16*, 2489.
[25] G. Park, W. Choi, J. Kim, Y. C. Choi, Y. H. Lee, C. Lim, *Cryst. Growth Des.* **2000**, *220*, 494.
[26] J. Q. Hu, Q. Li, X. M. Meng, C. S. Lee, S. T. Lee, *J. Phys. Chem. B* **2002**, *106*, 9536.
[27] G. Sinha, K. Adhikary, S. Chaudhuri, *Opt. Mater.* **2007**, *29*, 718.
[28] S. Music, S. Popovic, M. Ristic, *Mater. Lett.* **2005**, *59*, 1227.
[29] B. Geng, L. Zhang, G. Meng, T. Xie, X. Peng, Y. Lin, *Cryst. Growth Des.* **2003**, *259*, 291.
[30] K. Girija, *Semicond. Sci. Technol.* **2013**, *28*, 035015.
[31] H. S. Qian, P. Gunawan, Y. X. Zhang, G. F. Lin, J. W. Zheng, R. Xu, *Cryst. Growth Des.* **2008**, *8*, 1282.
[32] D. Li, *J. Mater. Chem. A* **2013**, *1*, 12417.
[33] Y. Hou, J. Zhang, Z. Ding, L. Wu, *Powder Technol.* **2010**, *203*, 440.
[34] J. Zhang, Z. Liu, C. Lin, J. Lin, *Cryst. Growth Des.* **2005**, *280*, 99.
[35] Y. Quan, D. Fang, X. Zhang, S. Liu, K. Huang, *Mater. Chem. Phys.* **2010**, *121*, 142.
[36] C. R. Patra, Y. Mastai, A. Gedanken, *J. Nanopart. Res.* **2004**, *6*, 509.
[37] X. Liu, G. Qiu, Y. Zhao, N. Zhang, R. Yi, *J. Alloys Compd.* **2007**, *439*, 275.
[38] T. Katona, *Nat. Photonics* **2008**, *2*, 77.
[39] H. Matsubara, *Science* **2008**, *319*, 445.
[40] X. H. Wang, L. W. Guo, H. Q. Jia, Z. G. Xing, Y. Wang, X. J. Pei, J. M. Zhou, H. Chen, *Appl. Phys. Lett.* **2009**, *94*, 2007.
[41] S. Strite, *J. Vac. Sci. Technol., B: Microelectron. Nanometer Struct. – Process., Meas., Phenom.* **1992**, *10*, 1237.

© 2023 The Authors. Advanced Photonics Research published by Wiley-VCH GmbH

26999293, 0, Downloaded from https://onlinelibrary.wiley.com/doi/10.1002/adpr.202300252 by Readcube (Labtiva Inc.), Wiley Online Library on [20/12/2023]. See the Terms and Conditions (https://onlinelibrary.wiley.com/terms-and-conditions) on Wiley Online Library for rules of use; OA articles are governed by the applicable Creative Commons License

[42] A. Avramescu, T. Lermer, J. Müller, S. Tautz, D. Queren, S. Lutgen, U. Strau, *Appl. Phys. Lett.* **2009**, *95*, 071103.
[43] M. Asif Khan, *Appl. Phys. Lett.* **1998**, *2917*, 3.
[44] C. J. Neufeld, N. G. Toledo, S. C. Cruz, M. Iza, S. P. DenBaars, U. K. Mishra, *Appl. Phys. Lett.* **2008**, *93*, 91.
[45] F. A. Ponce, D. P. Bour, *Nature* **1997**, *386*, 351.
[46] Z. Y. Al Balushi, K. Wang, R. K. Ghosh, R. A. Vilá, S. M. Eichfeld, J. D. Caldwell, X. Qin, Y. C. Lin, P. A. Desario, G. Stone, S. Subramanian, D. F. Paul, R. M. Wallace, S. Datta, J. M. Redwing, J. A. Robinson, *Nat. Mater.* **2016**, *15*, 1166.
[47] N. Sanders, D. Bayerl, G. Shi, K. A. Mengle, E. Kioupakis, *Nano Lett.* **2017**, *17*, 7345.
[48] M. A. Moram, M. E. Vickers, *Rep. Prog. Phys.* **2009**, *72*, 036502.
[49] T. Kuykendall, P. Pauzauskie, S. Lee, Y. Zhang, J. Goldberger, P. Yang, *Nano Lett.* **2003**, *3*, 1063.
[50] X. Chen, *Adv. Mater.* **2003**, *15*, 419.
[51] J. Goldberger, R. He, Y. Zhang, S. Lee, H. Yan, H. J. Choi, P. Yang, *Nature* **2003**, *422*, 599.
[52] A. Usui, *Jpn. J. Appl. Phys., Part 2* **1997**, *36*, 899.
[53] T. Sasaki, T. Matsuoka, *J. Appl. Phys.* **1988**, *64*, 4531.
[54] A. Zavabeti, J. Z. Ou, B. J. Carey, N. Syed, R. Orrell-Trigg, E. L. H. Mayes, C. Xu, O. Kavehei, A. P. O'Mullane, R. B. Kaner, K. Kalantar-Zadeh, T. Daeneke, *Science* **2017**, *358*, 332.
[55] T. Daeneke, K. Khoshmanesh, N. Mahmood, I. A. De Castro, D. Esrafilzadeh, S. J. Barrow, M. D. Dickey, K. Kalantar-Zadeh, *Chem. Soc. Rev.* **2018**, *47*, 4073.
[56] P. Aukarasereenont, A. Goff, C. Kim Nguyen, C. F. McConville, A. Elbourne, A. Zavabeti, T. Daeneke, *Chem. Soc. Rev.* **2022**, *51*, 1253.
[57] M. Martin, R. Dronskowski, J. Janek, K. D. Becker, D. Roehrens, J. Brendt, M. W. Lumey, L. Nagarajan, I. Valov, A. Börger, *Prog. Solid State Chem.* **2009**, *37*, 132.
[58] A. Goff, P. Aukarasereenont, C. K. Nguyen, R. Grant, N. Syed, A. Zavabeti, A. Elbourne, T. Daeneke, *Dalton Trans.* **2021**, *50*, 7513.
[59] K. A. Messalea, N. Syed, A. Zavabeti, A. Jannat, P. Aukarasereenont, C. K. Nguyen, M. X. Low, S. Walia, B. Haas, C. T. Koch, N. Mahmood, K. Khoshmanesh, K. Kalantar-zadeh, T. Daeneke, *ACS Nano* **2021**, *15*, 16067.
[60] A. Zavabeti, P. Aukarasereenont, H. Tuohey, N. Syed, A. Jannat, A. Elbourne, K. A. Messalea, B. Y. Zhang, B. J. Murdoch, J. G. Partridge, M. Wurdack, D. L. Creedon, J. van Embden, K. Kalantar-Zadeh, S. P. Russo, C. F. McConville, T. Daeneke, *Nat. Electron.* **2021**, *4*, 277.
[61] N. Syed, A. Zavabeti, K. A. Messalea, E. Della Gaspera, A. Elbourne, A. Jannat, M. Mohiuddin, B. Y. Zhang, G. Zheng, L. Wang, S. P. Russo, D. Esrafilzadeh, C. F. McConville, K. Kalantar-Zadeh, T. Daeneke, *J. Am. Chem. Soc.* **2019**, *141*, 104.
[62] N. Syed, A. Stacey, A. Zavabeti, C. K. Nguyen, B. Haas, C. T. Koch, D. L. Creedon, E. Della Gaspera, P. Reineck, A. Jannat, M. Wurdack, S. E. Bamford, P. J. Pigram, S. A. Tawfik, S. P. Russo, B. J. Murdoch, K. Kalantar-Zadeh, C. F. McConville, T. Daeneke, *ACS Nano* **2022**, *16*, 5476.
[63] R. S. Datta, N. Syed, A. Zavabeti, A. Jannat, M. Mohiuddin, M. Rokunuzzaman, B. Yue Zhang, M. A. Rahman, P. Atkin, K. A. Messalea, M. B. Ghasemian, E. Della Gaspera, S. Bhattacharyya, M. S. Fuhrer, S. P. Russo, C. F. McConville, D. Esrafilzadeh, K. Kalantar-Zadeh, T. Daeneke, *Nat. Electron.* **2020**, *3*, 51.
[64] K. A. Messalea, B. J. Carey, A. Jannat, N. Syed, M. Mohiuddin, B. Y. Zhang, A. Zavabeti, T. Ahmed, N. Mahmood, E. Della Gaspera, K. Khoshmanesh, K. Kalantar-Zadeh, T. Daeneke, *Nanoscale* **2018**, *10*, 15615.
[65] N. Syed, A. Zavabeti, J. Z. Ou, M. Mohiuddin, N. Pillai, B. J. Carey, B. Y. Zhang, R. S. Datta, A. Jannat, F. Haque, K. A. Messalea, C. Xu, S. P. Russo, C. F. McConville, T. Daeneke, K. Kalantar-Zadeh, *Nat. Commun.* **2018**, *9*, 3618.
[66] G. Schön, *J. Electron. Spectros. Relat. Phenom.* **1973**, *2*, 75.
[67] N. Elkashef, R. S. Srinivasa, S. Major, S. C. Sabharwal, K. P. Muthe, *Thin Solid Films* **1998**, *333*, 9.
[68] M. Wurdack, T. Yun, E. Estrecho, N. Syed, S. Bhattacharyya, M. Pieczarka, A. Zavabeti, S. Y. Chen, B. Haas, J. Müller, M. N. Lockrey, Q. Bao, C. Schneider, Y. Lu, M. S. Fuhrer, A. G. Truscott, T. Daeneke, E. A. Ostrovskaya, *Adv. Mater.* **2021**, *33*, 2005732.
[69] M. Wurdack, T. Yun, E. Estrecho, N. Syed, S. Bhattacharyya, M. Pieczarka, A. Zavabeti, S. Y. Chen, B. Haas, J. Müller, M. N. Lockrey, Q. Bao, C. Schneider, Y. Lu, M. S. Fuhrer, A. G. Truscott, T. Daeneke, E. A. Ostrovskaya, *Adv. Mater.* **2021**, *33*, 2005732.
[70] P. Motamedi, N. Dalili, K. Cadien, *J. Mater. Chem. C* **2015**, *3*, 7428.
[71] Z. Liu, T. Yamazaki, Y. Shen, T. Kikuta, N. Nakatani, Y. Li, *Sens. Actuators, B* **2008**, *129*, 666.
[72] J. T. Yan, C. T. Lee, *Sens. Actuators, B* **2009**, *143*, 192.
[73] M. F. Al-Kuhaili, S. M. A. Durrani, E. E. Khawaja, *Appl. Phys. Lett.* **2003**, *83*, 4533.
[74] P. Marie, X. Portier, J. Cardin, *Phys. Status Solidi A* **2008**, *205*, 1943.
[75] M. E. Lin, B. N. Sverdlov, S. Strite, H. Morkoc, A. E. Drakin, *Electron. Lett.* **1993**, *29*, 1759.
[76] H. Amano, N. Watanabe, N. Koide, I. Akasaki, *Jpn. J. Appl. Phys.* **1993**, *32*, L1000.
[77] G. Yu, H. Ishikawa, T. Egawa, T. Soga, J. Watanabe, T. Jimbo, M. Umeno, *Jpn. J. Appl. Phys., Part 2* **1997**, *36*, 2202.
[78] T. Kawashima, H. Yoshikawa, S. Adachi, S. Fuke, K. Ohtsuka, *J. Appl. Phys.* **1997**, *82*, 3528.
[79] G. Yu, H. Ishikawa, M. Umeno, T. Egawa, J. Watanabe, T. Jimbo, T. Soga, *Appl. Phys. Lett.* **1998**, *72*, 2202.
[80] T. Onuma, *Jpn. J. Appl. Phys.* **2016**, *55*, 1202B2.
[81] M. Rebien, *Appl. Phys. Lett.* **2016**, *250*, 10.
[82] A. Segura, L. Artús, R. Cuscó, R. Goldhahn, M. Feneberg, *Phys. Rev. Mater.* **2017**, *1*, 024604.
[83] A. You, M. A. Y. Be, I. In, *J. Appl. Phys.* **2020**, *686*, 77.
[84] J. W. Roberts, P. R. Chalker, B. Ding, R. A. Oliver, J. T. Gibbon, L. A. H. Jones, V. R. Dhanak, L. J. Phillips, J. D. Major, F. C. Massabuau, *J. Cryst. Growth* **2019**, *528*, 125254.
[85] A. R. A. Zauner, *Mater. Res.* **1999**, *2*, 419.
[86] E. S. Hellman, *Mater. Res.* **1999**, *2*, 1.
[87] P. Boher, in *Proc. 203rd Electrochemical Society Meeting*, Paris, 27 April–2 May **2003**, Symposium J2, p. 258.
[88] T. Yang, S. Goto, M. Kawata, K. Uchida, A. Niwa, J. Gotoh, *Jpn. J. Appl. Phys., Part 2* **1998**, *37*, L1105.
[89] A. Biswas, D. Bhattacharyya, N. K. Sahoo, B. S. Yadav, S. S. Major, *J. Alloys Compd.* **2008**, *103*, 083541.
[90] S. J. Yoo, Q. H. Park, *Nanophotonics* **2022**, *11*, 2811.
[91] S. Funke, U. Wurstbauer, B. Miller, A. Matković, A. Green, A. Diebold, C. Röling, P. H. Thiesen, *Appl. Surf. Sci.* **2017**, *421*, 435.
[92] F. K. Shan, G. X. Liu, W. J. Lee, G. H. Lee, I. S. Kim, B. C. Shin, *J. Appl. Phys.* **2005**, *98*, 023504.
[93] O. M. Bordun, I. Y. Kukharskyy, B. O. Bordun, V. B. Lushchanets, *J. Appl. Spectrosc.* **2014**, *81*, 771.
[94] S. Scandolo, P. Giannozzi, C. Cavazzoni, S. de Gironcoli, A. Pasquarello, S. Baroni, *Z. Kristallogr. – Cryst. Mater.* **2005**, *220*, 574.
[95] B. S. Zou, V. V. Volkov, Z. L. Wang, *Chem. Mater.* **1999**, *11*, 3037.
[96] J. Robertson, *Phys. Status Solidi B* **2008**, *245*, 1026.
[97] S. Poncé, *Phys. Rev. Res.* **2020**, *2*, 033102.
[98] H. Qin, *Materials* **2017**, *10*, 1419.
[99] L. A. Agapito, S. Curtarolo, M. B. Nardelli, *Phys. Rev. X* **2015**, *5*, 011006.
[100] Q. Yan, P. Rinke, A. Janotti, M. Scheffler, C. G. Van De Walle, M. Foundry, L. Berkeley, *Am. Phys. Soc.* **2014**, *1*, 125118.

© 2023 The Authors. Advanced Photonics Research published by Wiley-VCH GmbH

26999293, 0, Downloaded from https://onlinelibrary.wiley.com/doi/10.1002/adpr.202300252 by Readcube (Labtiva Inc.), Wiley Online Library on [20/12/2023]. See the Terms and Conditions (https://onlinelibrary.wiley.com/terms-and-conditions) on Wiley Online Library for rules of use; OA articles are governed by the applicable Creative Commons License

[101] D. Mora-Fonz, *Adv. Electron. Mater.* **2020**, *6*, 1900760.
[102] J. P. Perdew, K. Burke, M. Ernzerhof, *Phys. Rev. Lett.* **1996**, *77*, 3865.
[103] M. Schlipf, F. Gygi, *Comput. Phys. Commun.* **2015**, *196*, 36.
[104] A. Calzolari, M. B. Nardelli, *Sci. Rep.* **2013**, *3*, 2999.
[105] P. Gopal, M. Fornari, S. Curtarolo, L. A. Agapito, L. S. I. Liyanage, M. B. Nardelli, *Phys. Rev. B: Condens. Matter Mater. Phys.* **2015**, *91*, 245202.
[106] A. Calzolari, A. Ruini, A. Catellani, *ACS Photonics* **2014**, *1*, 703.
[107] M. Passlack, E. F. Schubert, W. S. Hobson, M. Hong, N. Moriya, S. N. G. Chu, K. Konstadinidis, J. P. Mannaerts, M. L. Schnoes, G. J. Zydzik, *J. Appl. Phys.* **1995**, *77*, 686.
[108] M. Rebien, W. Henrion, M. Hong, J. P. Mannaerts, M. Fleischer, *Appl. Phys. Lett.* **2002**, *81*, 250.
[109] A. Ortiz, J. C. Alonso, E. Andrade, C. Urbiola, *J. Electrochem. Soc.* **2001**, *148*, F26.
[110] A. R. A. Zauner, M. A. C. Devillers, P. R. Hageman, P. K. Larsen, S. Porowski, *Mater. Res.* **1998**, *3*, e17.

© 2023 The Authors. Advanced Photonics Research published by Wiley-VCH GmbH

26999293, 0, Downloaded from https://onlinelibrary.wiley.com/doi/10.1002/adpr.202300252 by Readcube (Labtiva Inc.), Wiley Online Library on [20/12/2023]. See the Terms and Conditions (https://onlinelibrary.wiley.com/terms-and-conditions) on Wiley Online Library for rules of use; OA articles are governed by the applicable Creative Commons License